The Fate of North Atlantic Subtropical Mode Water in the FLAME Model

S. F. GARY AND M. S. LOZIER

Duke University, Durham, North Carolina

Y.-O. KWON

Woods Hole Oceanographic Institution, Woods Hole, Massachusetts

J. J. PARK

Kyungpook National University, Sangju, South Korea

(Manuscript received 19 September 2013, in final form 20 December 2013)

ABSTRACT

North Atlantic Subtropical Mode Water, also known as Eighteen Degree Water (EDW), has the potential to store heat anomalies through its seasonal cycle: the water mass is in contact with the atmosphere in winter, isolated from the surface for the rest of the year, and reexposed the following winter. Though there has been recent progress in understanding EDW formation processes, an understanding of the fate of EDW following formation remains nascent. Here, particles are launched within the EDW of an eddy-resolving model, and their fate is tracked as they move away from the formation region. Particles in EDW have an average residence time of ~10 months, they follow the large-scale circulation around the subtropical gyre, and stratification is the dominant criteria governing the exit of particles from EDW. After sinking into the layers beneath EDW, particles are eventually exported to the subpolar gyre. The spreading of particles is consistent with the large-scale potential vorticity field, and there are signs of a possible eddy-driven mean flow in the southern portion of the EDW domain. The authors also show that property anomalies along particle trajectories have an average integral time scale of ~3 months for particles that are in EDW and ~2 months for particles out of EDW. Finally, it is shown that the EDW turnover time for the model in an Eulerian frame (~3 yr) is consistent with the turnover time computed from the Lagrangian particles provided that the effects of exchange between EDW and the surrounding waters are included.

1. Introduction

Mode waters are large volumes of near-surface waters with significantly more uniform properties, and thus less vertical stratification, than the surrounding water masses (Hanawa and Talley 2001). One of these mode waters, North Atlantic Subtropical Mode Water, also known as Eighteen Degree Water (EDW), occupies a significant fraction of the total volume of the upper thermocline waters and is identified by its mode temperature of ~18°C (Worthington 1958; Joyce 2012). EDW is created south of the Gulf Stream during winter convective events that involve strong fluxes of heat from the ocean to the atmosphere (Worthington 1958). In fact, some of the strongest ocean-to-atmosphere surface heat fluxes in the global ocean are involved in the production of EDW (Grist and Josey 2003; Large and Yeager 2009). Studies have quantified EDW production via volume inventories (Kwon and Riser 2004), with air–sea fluxes (Speer and Tziperman 1992; Maze et al. 2009), and with a merger of both approaches (Forget et al. 2011).

The substantial volume of EDW has the potential to be a reservoir of anomalous heat and thus maintain a memory of the previous years' air–sea interaction. Given the intense air–sea fluxes and deep mixed layer associated with EDW formation, EDW heat content anomalies could feed back onto subsequent years' winter air–sea interaction and mixed layer properties via reoutcropping (Kwon and Riser 2004; Dong et al. 2007; Kelly et al. 2010). Furthermore, low nutrient concentrations within EDW may affect the subsurface nutrient reservoir in the

Corresponding author address: Stefan Gary, Division of Earth and Ocean Sciences, Duke University, Box 90227, Durham, NC 27708.
E-mail: stefan.gary@duke.edu; stefan.gary@sams.ac.uk

DOI: 10.1175/JPO-D-13-0202.1

subtropical North Atlantic, potentially impacting biogeochemical cycling on the gyre scale (Palter et al. 2005).

Despite recent progress on EDW formation (Joyce et al. 2009; Davis et al. 2013; Silverthorne and Toole 2013), there is comparatively little information about the fate of EDW. Fratantoni et al. (2013) tracked the movement of EDW columns with 40 profiling floats for ~3 yr. In addition to mapping the EDW flow field and layer thickness, Fratantoni et al. (2013) directly observed strong eddies within EDW and found that EDW parcels are reexposed to the atmosphere on time scales of less than a year. This outcropping time scale is surprising in light of previous studies concluding that the average EDW turnover time scale is at least a couple years (Jenkins 1988; Kwon and Riser 2004). However, it is important to note that EDW reemergence is not necessarily related to EDW turnover; reemergence quantifies how quickly EDW is reexposed to the atmosphere, while the turnover time is an estimate of how long it takes to replace the entire volume of EDW based on the rates of EDW production and destruction.

In this paper, we focus on the fate and export of EDW through the lens of 25-yr Lagrangian particle trajectories simulated within a high-resolution ocean model. We use an ensemble of simulated trajectories to answer the following questions about the fate of particles initially launched in EDW: Where and when do particles exit and reenter EDW? Where do particles go as they circulate within EDW? Where do particles go after they exit EDW? What are differences between the EDW and non-EDW pathways? Finally, what is the persistence of anomalies along particle trajectories?

After presenting details about the observations, model, and methods used in this work (section 2), we compare the turnover times and spatial distribution of EDW in both observations and the model in an Eulerian frame (section 3). In section 4, we present the exits and entries of particles from EDW, the pathways followed by the particles, the large-scale dynamical constraints on the particles, and the integral and turnover time scales derived from the particle trajectories. Section 5 contains a summary and our conclusions.

2. Methods

a. Sources and processing of hydrographic data

We created a North Atlantic hydrographic database using all profiles that had both temperature and salinity in the *World Ocean Database* (*WOD*) available in June 2012 (National Oceanographic Data Center 2012). This database, which includes data from bottle, CTD, and Argo floats archived in the *WOD*, was quality controlled and then used to construct two-dimensional gridded fields from the profile data, following the specifications of Lozier et al. (1995). The median date of the profiles was 1988. Of the 469 653 original profiles, 403 041 profiles satisfied the quality control filters and are used here.

b. Description of the FLAME model

The ocean general circulation model output analyzed in this paper is from the eddy-resolving member of the Family of Linked Atlantic Model Experiments (FLAME) (Böning et al. 2006; Hüttl-Kabus and Böning 2008; Biastoch et al. 2008) based on a modified version of the Modular Ocean Model, version 2 (MOM2; Pacanowski 1996). The model domain was a $^1/_{12}°$ horizontal resolution Mercator grid spanning 18°S–70°N with open boundary conditions at the southern and northern boundaries. The model was discretized on 45 vertical levels with a spacing of 10 m near the surface, increasing to a maximum of 250 m below 2000 m. In the upper 500 m, close to the maximum depth of EDW, the maximum vertical spacing was 70 m. The model was initialized at rest with January climatological temperature and the salinity anomalies of Levitus et al. (1994) and Levitus and Boyer (1994), superimposed on the annual means of Boyer and Levitus (1997). The model was spun up for 10 yr with European Centre for Medium-Range Weather Forecasts (ECMWF) climatological forcing. For the 1990–2004 hindcast simulation, the model was forced with interannual anomalies based on the National Centers for Environmental Prediction–National Center for Atmospheric Research (NCEP–NCAR) reanalysis (Kalnay et al. 1996) added to the climatological forcing used during spinup. Snapshots of the velocity and tracer fields at regular 3-day intervals and in monthly-mean fields were stored; a monthly climatology was constructed from the latter fields. It has been shown that the FLAME model output compares favorably with eddy kinetic energy (EKE) derived from altimeters and surface drifters (Burkholder and Lozier 2011), as well as observed Lagrangian pathways of the deep limb of the Atlantic meridional overturning circulation and observed intermediate depth potential vorticity fields (Gary et al. 2011).

c. Definition of EDW

EDW is usually defined by a temperature T range of 17.0°–19.0°C, with additional constraints on stratification to ensure a focus on the thermostad or minimum potential vorticity layer (Joyce 2012). Examples of additional filtering are the exclusion of waters east of the Mid-Atlantic Ridge (Worthington 1976) or 35°W (Kwon and Riser 2004) to remove Madeira Mode Water (Siedler et al. 1987) and the imposition of a limit on the stratification

based on the vertical temperature gradient (e.g., Klein and Hogg 1996; Alfultis and Cornillon 2001; Kwon and Riser 2004) or potential vorticity q (e.g., Talley and Raymer 1982; Klein and Hogg 1996; Forget et al. 2011).

Here, we use the Kwon and Riser (2004) EDW definition with a slight modification suited to the FLAME simulation. We use the stratification limit based on $\partial T/\partial z$ rather than q or the vertical density gradient in order to more easily compare with observations (e.g., Kwon and Riser 2004; Fratantoni et al. 2013). Y.-O. Kwon et al. (2014, unpublished manuscript) compare observed and modeled vertical sections at 52°W and conclude that EDW in FLAME is best defined as water from 17.0° to 20.0°C and with $\partial T/\partial z \leq 0.01°C\,m^{-1}$. Briefly, the vertical stratification in the core of the modeled EDW is slightly higher than the observations, thus shifting the vertical temperature gradient from 0.006° to $0.01°C\,m^{-1}$. Because the model exhibits lower temperature stratification than observations in the range of 19.0°–20.0°C, Y.-O. Kwon et al. (2014, unpublished manuscript) decided to include these warmer waters within the definition of EDW, shifting the traditional upper bound of 19.0° to 20.0°C. The 17.0°–20.0°C and $\partial T/\partial z \leq 0.01°C\,m^{-1}$ definition of EDW is applied throughout this study to the FLAME model output. Finally, we chose to filter out thin, temporary layers of EDW by requiring that the EDW layer must be at least 50 m thick.

d. *Particle launch strategy in FLAME*

To track the movement of EDW, we seeded the FLAME model on a 1° × 1° × 20 m grid west of 35°W (Fig. 1). At each grid node and each depth within EDW, two adjacent particles were launched with a horizontal separation of 1/12°. The adjacent particles were launched close together to allow for dispersion calculations, which are not discussed here. Each year from 1990 to 1999, particles were launched from the grid 6 times at 12-day intervals from 15 February to 15 April. We further restricted our analysis to the 775 045 EDW particles that were launched, at all depths, within a column of EDW in contact with the sea surface.

e. *Computation of particle trajectories in FLAME*

Following the EDW particle launch, particle trajectories were computed for 25 yr from snapshots of the model velocity field updated every 3 days from 1990 to 2004. We used an Euler scheme with an adaptive time step to integrate the velocity field. This technique was based on the sensitivity analysis of Böning and Cox (1988) and was described in detail by Gary et al. (2011). Furthermore, Gary et al. (2011) showed that including higher temporal resolution does not have a significant impact on the spreading of the trajectory ensemble. We computed trajectories offline with stored output of the model rather than during the model run because this allowed recycling of the velocity fields with a single temporal discontinuity between 31 December 2004 and 1 January 1990. The reuse of velocity fields allowed for the extension of trajectory simulations beyond the 15 yr of available model output.

Linear interpolation in time and space was used to determine the velocity, temperature, salinity, vertical temperature gradient, and vertical density gradient for

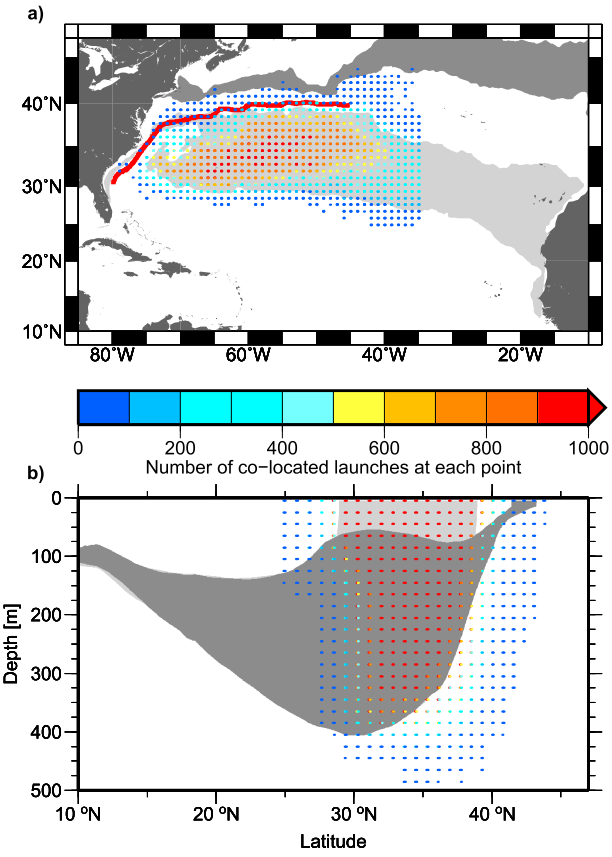

FIG. 1. EDW in the FLAME model and particle launch locations. (a) Map of particle launch locations (colored dots), region between the mean 17°–20°C sea surface isotherms for March (light gray) and September (dark gray) in the FLAME model. The red line is the north wall of the Gulf Stream determined by the average position of the 15°C isotherm at 200 m west of 45°W (Fuglister and Voorhis 1965). (b) The same particle launch positions are shown in a vertical section along with the region between the climatological-mean 17°–20°C isotherms for March (light gray) and September (dark gray). The isotherms in (b) are taken from the March or September monthly climatology computed from the 1990–2004 FLAME output and are zonally averaged from 70° to 35°W. The color of each launch position indicates the number of particles that are launched at each (x, y) or (y, z) position. All particles satisfy the EDW definition for FLAME (section 2c), and the EDW layer is outcropped at the instant of launch.

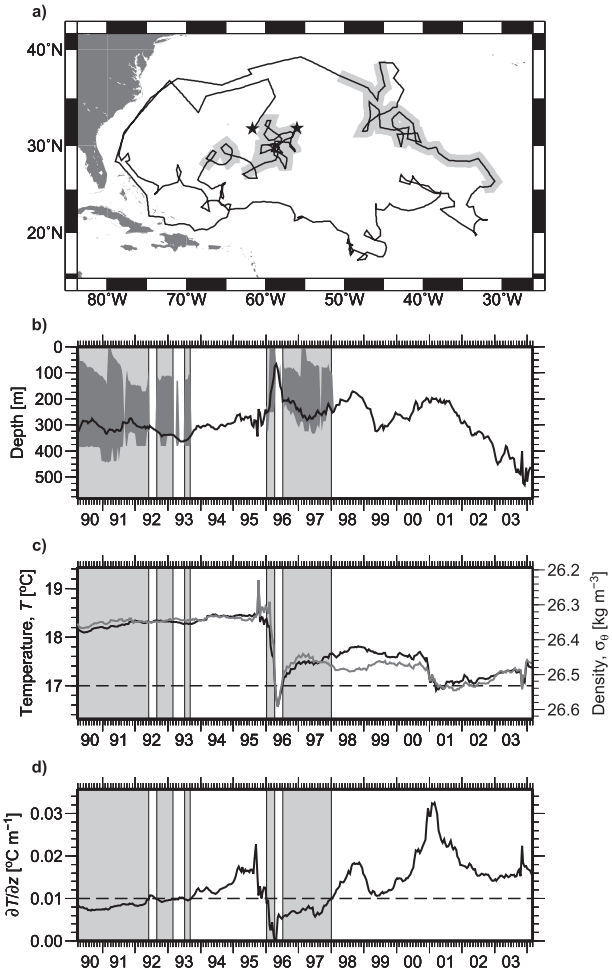

FIG. 2. Example of a particle trajectory. (a) Map of the particle positions. The particle was launched at the black star near 30°N, 55°W. (b) Lagrangian time series of particle depth. Dark gray shading indicates the EDW layer containing the particle. (c) Time series of potential temperature (black) and potential density (gray) along the particle track. The horizontal dashed lines are the EDW temperature limits (17°–20°C). (d) Time series of the vertical gradient in potential temperature along the particle track. The horizontal dashed line is the vertical stratification limit ($0.01°C\,m^{-1}$). Light gray shading indicates the duration of the EDW segments of the particle (section 2f). All lines are plotted at 15-day resolution.

each particle. These Lagrangian data, along with the corresponding particle positions and date, were stored every 15 days over the 25-yr simulation. After the trajectories were computed, the upper and lower bounds of the EDW layer containing each particle, if present, were determined from the model fields using the same linear interpolation used to calculate the other properties at each particle position.

An example of one particle trajectory is presented in Fig. 2. The particle was launched in outcropped EDW in March 1990 and slowly moved to the southeast while staying inside EDW for ~2 yr. The particle exited EDW due to the increasing stratification, experienced a series of shorter EDW reentry and exit events, followed the large-scale anticyclonic circulation of the subtropical gyre, and then entered the Gulf Stream. While in the Gulf Stream in winter, the particle reentered EDW for ~3 months following a very strong cooling event, exited due to its low temperature, reentered, and recirculated for ~18 months within EDW, and then exited again. This last exit was due to an increase in stratification.

f. Sorting particle trajectories into EDW and non-EDW segments

As shown in Fig. 2, it is possible for a particle to be launched in EDW and then exit and reenter the water mass. Particle trajectories were subdivided into EDW and non-EDW segments that each lasted for more than 1 month, increasing the size of the trajectory ensemble at almost no computational cost. Although there were a total of $\sim 4 \times 10^6$ EDW and non-EDW segments shorter than 1 month, they were not included in this analysis because they do not contribute to the longer-term fate of EDW. One such segment is shown in Fig. 2 near April 1993. Removing all segments less than 1 month left 3.49×10^6 EDW and 3.61×10^6 non-EDW segments.

EDW and non-EDW segments were further grouped into temporary and permanent categories. We defined a temporary segment to be an EDW or non-EDW segment whose endpoint coincides with a detected exit or entrance. For example, the gray bands in Fig. 2 highlight the temporarily in EDW segments for that particle trajectory. Also, the white band from mid-1993 to early 1996 is a temporarily out EDW segment. If the simulation were limited to the ~14 yr shown on the plot, the last segment, starting at the end of 1997, would correspond to a non-EDW segment whose true endpoint is unknown because the simulation ended before an EDW entrance was detected. This last segment would be classified as permanently out. Thus, for the full 25-yr simulation, the EDW and non-EDW segments were sorted into temporarily in (3.47×10^6), permanently in (1.54×10^4), temporarily out (2.86×10^6), and permanently out (7.51×10^5) segments. The number of permanently out segments is close to the number of original trajectories, indicating that almost all (~97%) of the original trajectories were simulated long enough to end outside of EDW. There was a total of 7.67×10^5 permanently in and permanently out segments that are each longer than 1 month. This sum was ~1% less than the total number of trajectories because we ignored the small number of permanently in or out segments that were less than 1-month long.

These segments were used to determine an inventory of EDW exit and entrance events. The last point of the

temporarily in EDW segments defined the locations of the EDW exit events. Similarly, the last point of each temporarily out EDW segment defined an EDW entrance event. In our inventory of EDW entrances, we ignored any of the initial launch locations because the launch of a particle is an imposed initial condition, not an entrance into EDW.

Finally, the temporal discontinuity from 31 December 2004 to 1 January 1990, which occurs when the 15 yr of model output are recycled to extend the simulation from 15 to 25 yr, was less than ideal because it had the potential to create false gradients in the model velocity and property fields at the instant of the temporal discontinuity, thus generating false EDW exits and entries. Therefore, all exits and entries that were within ±15 days of the temporal discontinuity were removed reducing the number of exits (entrances) from 3.47×10^6 (2.86×10^6) to 3.43×10^6 (2.83×10^6). Furthermore, the EDW and non-EDW segments that span the discontinuity were also removed, leaving 3.34×10^6, 1.34×10^4, 2.61×10^6, and 1.12×10^5 temporarily in, permanently in, temporarily out, and permanently out segments, respectively, in the data used for the Lagrangian analysis. This filtering effectively shortened the maximum length of the analysis from 25 to 15 yr because any segments longer than the 15 continuous years from 1990 to 2004 were discarded. The advantage to running 25-yr trajectories in the first place and then filtering the ensemble of segments is that the EDW in FLAME was sampled many more times than the original number of particle launch points. Furthermore, the analysis presented in this manuscript, using the 15-yr limited and filtered ensemble, was also carried out with the unfiltered 25-yr dataset (not shown), and the results are very similar, regardless of the 15- or 25-yr time limit.

3. An Eulerian perspective of EDW

The turnover time of EDW is computed by dividing the volume of EDW by the annual production or destruction rate of the water mass. Kwon and Riser (2004) estimate an observed EDW turnover of 3.57 ± 0.54 yr by dividing the total volume of EDW by the annual production of EDW. Using FLAME data, the average EDW volume of $12.48 \pm 1.61 \times 10^{14}$ m^3 divided by the annual formation ($3.93 \pm 1.21 \times 10^{14}$ m^3) results in an EDW turnover time of 3.18 ± 1.06 yr, consistent with the observed turnover time.

The distributions of EDW and non-EDW are shown in Fig. 3. The majority of the observed EDW is found in an approximately 1000-km-wide band south of the Gulf Stream, from about 25° to 40°N and 75° to 40°W. However, there are occasional stations at which no EDW is detected within that region. Similarly, EDW is sometimes detected outside of that region. Although the spatial distribution of EDW in FLAME is slightly different from the observed EDW (Fig. 3), a similar pattern

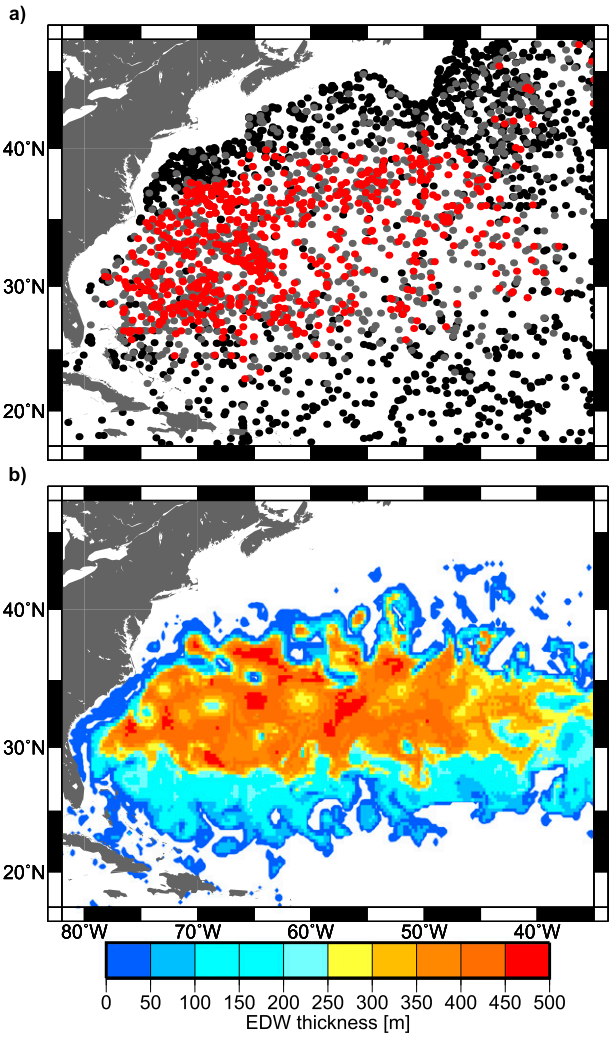

FIG. 3. The distribution of EDW and non-EDW. (a) Map of profile locations where no EDW (black dots), a less than 50-m-thick layer of EDW (gray dots), and an EDW layer thicker than 50 m (red dots) is found. Profiles are from the quality-controlled observational hydrographic database. All profiles used in this figure have a shallowest measurement of at least 100 m and a deepest measurement greater than 700 m (2.42×10^5 stations in our database satisfy this requirement). Each profile is linearly interpolated onto a 1-dbar vertical axis, and any values with $17° \le T \le 19°$C and $\partial T/\partial z \le 0.006°\text{C m}^{-1}$ are classified as EDW. The vertical temperature gradient is calculated as the slope of the linear regression between depth and temperature over a 20-m moving window centered at each depth. The stations are then sorted into those with no EDW (2.05×10^5 stations), only a layer thinner than 50 m (1.60×10^4 stations), and a layer thicker than 50 m (2.13×10^4 stations). For clarity, we limit the plot to every thirtieth station from each of these three classifications. (b) Thickness of EDW in FLAME, using the EDW definition of $17° \le T \le 20°$C and $\partial T/\partial z \le 0.01°\text{C m}^{-1}$, for the snapshot of the model output from 16 Mar 2004.

TABLE 1. Inventory of EDW exits and entries. The four constraints that are used to define EDW are $T \geq 17.0°C$, $T \leq 20.0°C$, $\partial T/\partial z \leq 0.01°C\,m^{-1}$, and EDW layer thickness greater than or equal to 50 m (layer). Exit or entry types in with an asterisk correspond to when exactly one of the four constraints is broken (met) for an exit (entrance). The exit or entry types without an asterisk are when more than one constraint plays a role in the EDW exit or entry. The two temperature constraints are always mutually exclusive.

Exit or entry type	No. exits	% Exits	No. entries	% Entries
$T < 17°C$ only*	231 615	6.75	107 725	3.81
$T < 17°C$ and layer	4900	0.14	4975	0.18
$T < 17°C$ and $\partial T/\partial z$	13 095	0.38	25 388	0.90
$T < 17°C$ and $\partial T/\partial z$ and layer	404	0.01	581	0.02
$T > 20$ only*	23 849	0.70	303 504	10.72
$T > 20°C$ and layer	1070	0.03	3866	0.14
$T > 20°C$ and $\partial T/\partial z$	40 913	1.19	149 204	5.27
$T > 20°C$ and $\partial T/\partial z$ and layer	529	0.02	883	0.03
$\partial T/\partial z$ only*	2 117 132	61.75	1 799 040	63.56
$\partial T/\partial z$ and layer	92 270	2.69	71 658	2.53
Layer only*	903 661	26.36	364 863	12.89
Total	3 428 797		2 830 346	

is observed in both observations and the model: patches of non-EDW appear within the EDW pool, while isolated observations of EDW lie outside the region. From the snapshot of the FLAME model EDW thickness, it appears that mesoscale eddies are responsible for these anomalous patches (Fig. 3).

4. Lagrangian pathways of EDW

a. EDW transformation

In this section we investigate where, when, and how particles exit from EDW. The classical interpretation of the EDW life cycle is that it is formed in winter, subducted, and then eroded by mixing into the surrounding waters during the rest of the year (e.g., Forget et al. 2011; Davis et al. 2013).

EDW exit and entrance events are classified into which EDW constraint the particles break (meet) in order to exit (enter) EDW. Because our definition of EDW consists of four constraints, particles can exit EDW by breaking one constraint: cooling to less than 17°C, warming above 20°C, increasing stratification to more than $0.01°C\,m^{-1}$, or by experiencing an EDW layer thickness of less than 50 m. In contrast to the exits, a particle makes its entry into EDW once it satisfies all four constraints: warming to 17°C, cooling to 20°C, decreasing stratification to $0.01°C\,m^{-1}$, or its EDW layer thickness growing to at least 50 m. Of course, it is also possible for particles to break (meet) more than one of the EDW constraints during exit (entrance). The 11 possible exit and entry types are listed in Table 1 along with the number of events detected for each type.

We examined a small number of isolated exit and entrance events (not shown), and these events appeared to be fully consistent with both large- and small-scale features in the model velocity and tracer fields surrounding the particle. The movement and properties of the particles can be attributed to the advection, mixing, and dissipation resolved and/or parameterized in the model. Although the trajectory calculation itself does not explicitly include mixing or dissipation, it is inevitable that the accumulation of small numerical errors due to interpolation and integration can introduce numerical dissipation. Nevertheless, on the time scales of particle entry and exit, usually a few months, it appears that the particles are accurately responding to the model velocity and tracer fields. This observation is consistent with the sensitivity study of the trajectory calculation presented in Gary et al. (2011).

There are fewer EDW entrance events than EDW exits because particles eventually move away from the EDW region over the course of the simulation and no new EDW particles are introduced to compensate for particles exported out of the subtropical gyre. The vast majority of exit and entry events are due to changes in stratification. The layer thickness constraint is the next most common constraint that is broken (met) for EDW exit (entry) events. Thickness and stratification together account for ~90% (~80%) of EDW exit (entry) events. Although there are exit and entry events where multiple EDW constraints are simultaneously broken (met), these events are a relatively minor contribution to the overall inventory of exits and entries. Finally, it is interesting to note that entrances and exits by cooling significantly outnumber entrances and exits by warming, consistent with the net annual surface heat flux out of EDW when it is in contact with the atmosphere.

Most of the EDW losses by cooling occur in the northeastern corner of the EDW pool, near 40°N, 40°W (Fig. 4a). This region is where the isotherms that define EDW experience a large meridional seasonal migration

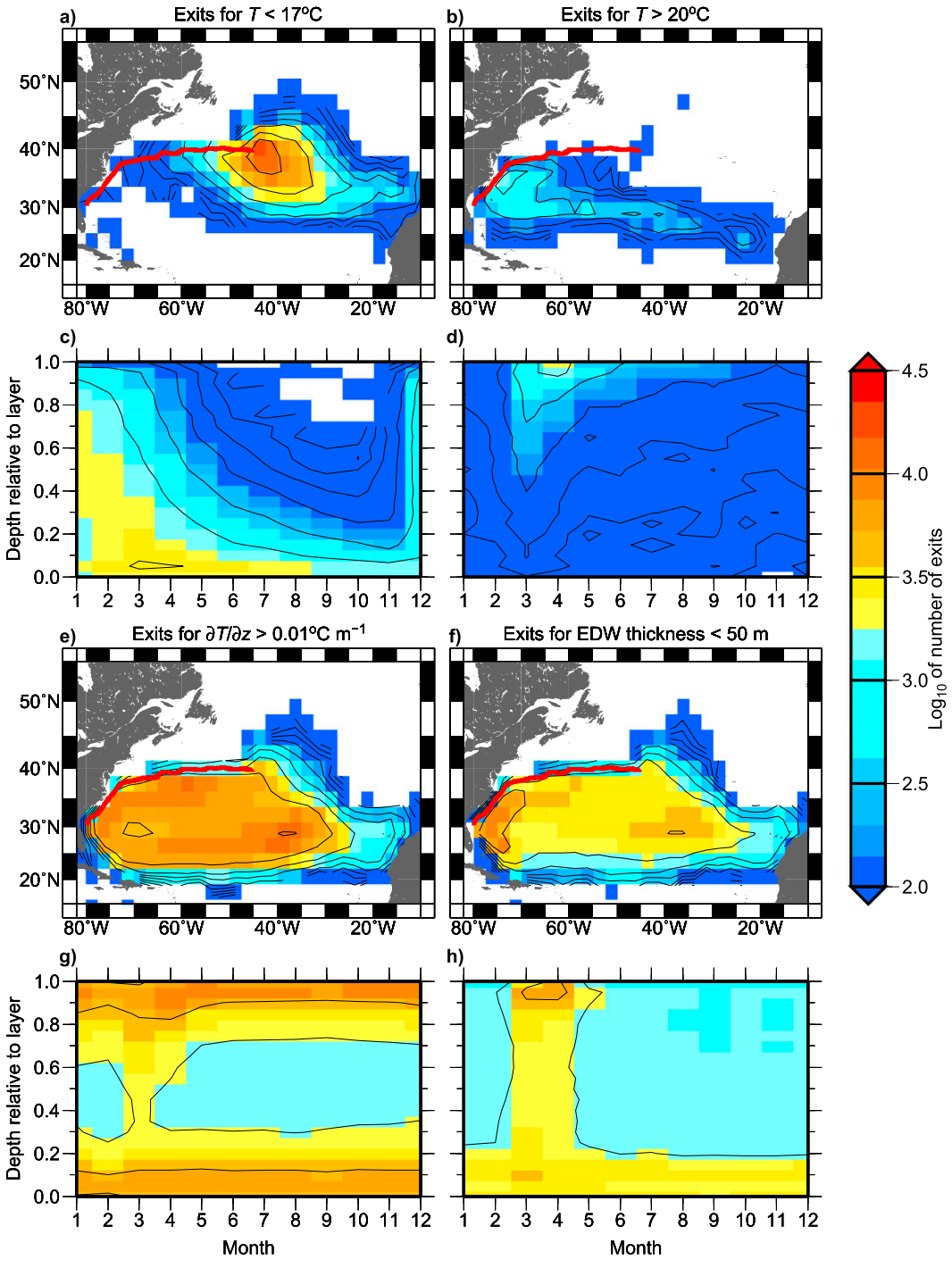

FIG. 4. Exits from EDW in FLAME. Histogram maps of EDW exits by (a) cooling, (b) warming, (e) increases in stratification, and (f) decreases in layer thickness. All exit positions for all months are binned onto a 2.5° × 2.5° grid. Monthly climatologies of the number of exit positions by (c) cooling, (d) warming, (g) stratification increases, and (h) decreases in layer thickness are also plotted with respect to month and the relative depth of particles within the EDW layer. The relative depth of the particle is defined as the difference between the bottom of the EDW layer and the depth of the particle divided by the total thickness of the EDW layer. Therefore, a relative depth of 0 corresponds to a particle at the bottom of the EDW layer, and a value of 1 is a particle near the top of the EDW layer. This normalization allows for particle exits within EDW layers of different thicknesses and absolute depths to be more easily compared. Particle exits are binned into 12 monthly bins and 0.05-wide relative depth bins. Color shading is the $\log_{10}$ of the number of exits in each bin, thus representing the order of magnitude of the number of exits at each location. Black contour lines are drawn at 0.5 intervals on the $\log_{10}$ scale. The red line in the maps is the time-mean position of the north wall of the Gulf Stream, as in Fig. 1.

within the mixed layer (Fig. 1), allowing EDW to either mix with colder waters or experience atmospheric cooling and thus exit the EDW temperature range by cooling. The seasonal cycle of EDW exits relative to depth within the EDW layer (Fig. 4c) indicates that most of the EDW exits by cooling occur in the winter at all depths within the EDW layer, with more exits toward the bottom of the layer, as particles are cooled by the atmosphere and sink or mix laterally. During the rest of the year, there are fewer, but persistent EDW exits by cooling, limited to the bottom of the EDW layer where EDW is eroded by mixing with the underlying colder waters. On the other end of the EDW temperature range, EDW loss events due to warming are concentrated in the western side of the EDW pool (Fig. 4b) where EDW is in close proximity to the warm waters advected northward by the Gulf Stream. EDW exits due to warming are primarily confined to the spring and summer when the upper portion of EDW is restratified by seasonal warming (Fig. 4d).

The majority of EDW exit events (~62%) are due to an increase in stratification. These exits occur throughout the EDW pool (Fig. 4e) with slightly higher concentrations of exits where EDW thins along the southern rim of the EDW pool and near the Gulf Stream (Fig. 1). EDW exits by stratification are similar to exits by temperature in that most exits occur near the top and bottom of the EDW layer (Fig. 4g). The EDW exits by stratification are fewest in February when the water column is destratifying and largest at the end of the winter when the upper portion of the EDW is restratifying. Because the minimum layer thickness constraint is similar to the stratification constraint, it is not surprising that the exits due to thin EDW layers (Figs. 4f,h) exhibit very similar spatial and seasonal patterns as the exits by stratification (Figs. 4e,g). The biggest difference between these two exit cases lies at the top of the EDW layer: aside from the end of winter when the upper water column is restratifying, particles rarely exit due to thin EDW layers near the top of the layer but particles can exit EDW near the top of the layer due to changes in stratification. This contrast suggests that during summer and autumn, the thickness of the EDW layer is relatively stable, but it is still possible for particles near the top of the EDW layer to experience changes in stratification while particles continue to exit near the bottom throughout the year.

The locations of EDW entrances (Fig. 5) are broadly similar to the locations of EDW exits (Fig. 4). In particular, there are similar large-scale features in the distributions of exits by cooling and entrances by warming, exits by warming and entrances by cooling, and exits and entrances due to stratification. These similarities suggest that there is exchange across the temperature and stratification limits that separate EDW from the surrounding waters. Furthermore, the exchange between EDW and non-EDW is compatible with the observation that single particles can exit and reenter EDW several times.

The annual cycles of EDW entries highlight the mechanisms that transform non-EDW into EDW. EDW entries by cooling, stratification, and layer thickness criteria have annual cycles dominated by the production of EDW in winter by atmospheric cooling, destratification, and the deepening of the mixed layer (Fig. 5). However, through the course of the whole annual cycle, there are many EDW entries along the bottom of the EDW layer (Figs. 5c,g,h), suggesting that particles from the underlying colder waters enter warmer EDW by isopycnal or diapycnal mixing over the course of the year. As with EDW exits, the annual cycle of EDW entrances by stratification shows consistently high rates of transformation at the upper and lower boundaries of EDW, but entrances due to layer thickness are rare in the upper portion of EDW. Finally, although we detect particle entries into EDW throughout the year (Figs. 5c,d,g,h), a sum over all exit/entry types shows that there are more exits than entrances at all depths in the EDW layer from April to November and vice versa from December to March. Therefore, although there are signs of year-round mixing at the top and bottom of the EDW layer, there is a net input of particles to EDW in the winter and a net loss during the rest of the year.

b. EDW pathways

In this section we examine the long-term fate of particles within and outside of the EDW pool by binning all EDW and non-EDW segment positions (Figs. 6 and 7, respectively) in four ensembles: permanently in, temporarily in, permanently out, and temporarily out. For each ensemble, we use the average of all particle positions at each time to produce ensemble trajectories, which are plotted on top of the histograms in Figs. 6 and 7. The temperature, density, and stratification along the ensemble-mean trajectories are also computed by averaging the corresponding properties over all particles at each time step.

The time dimension in Figs. 6 and 7 is the Lagrangian age of a segment: all segments' initial time is set to zero at the first point regardless of the year, season, or the original trajectory from which the segment was drawn. For EDW segments, the first point is the same as the point of entry into EDW, and for non-EDW segments, the first point is the point of exit from EDW. Because the length of a segment depends on the amount of time each segment resides in EDW, the total duration of each segment is not constant from segment to segment. Furthermore, the number of segments that contribute to the ensemble-average trajectory slowly decreases with time

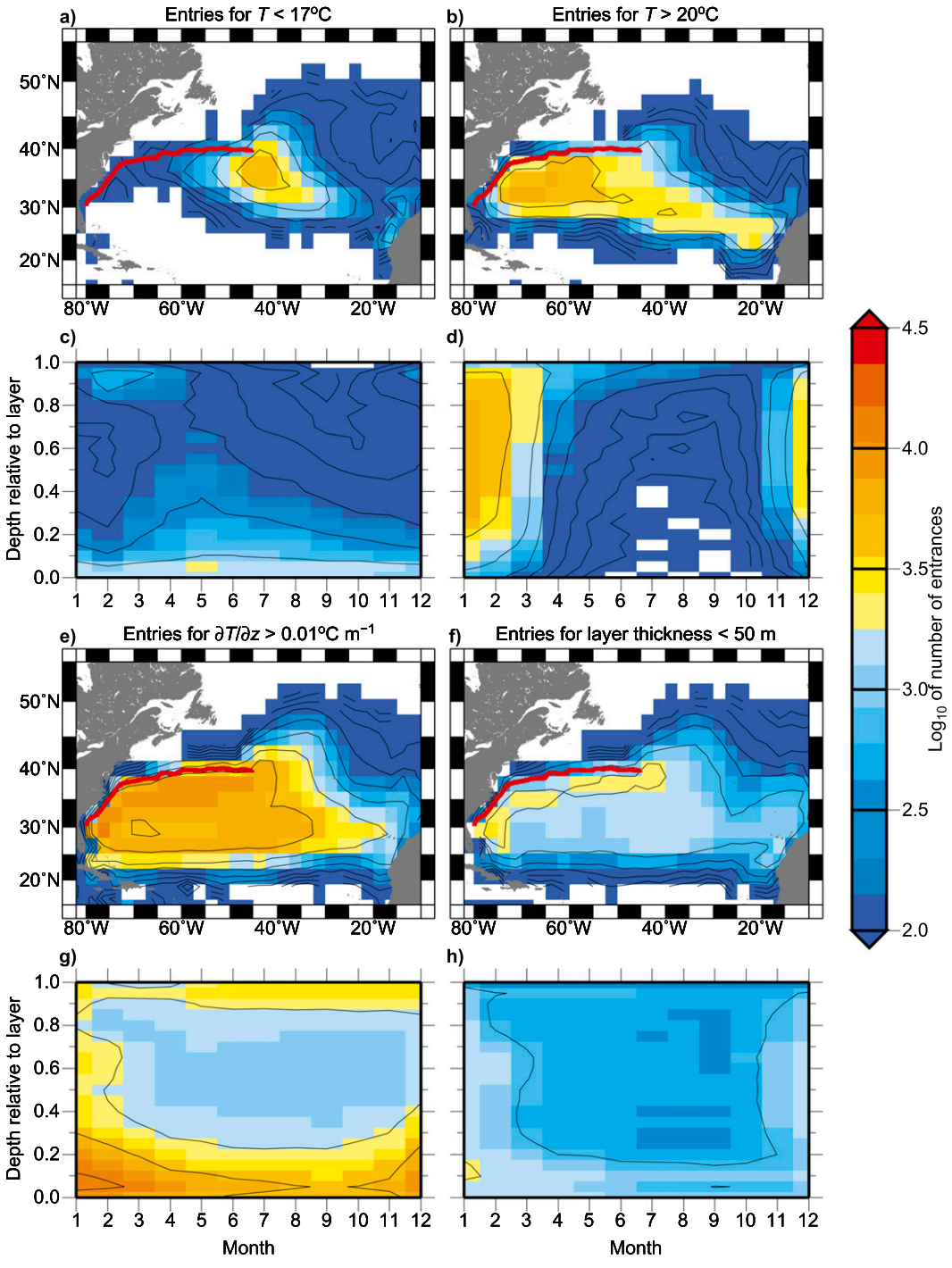

FIG. 5. Entrances into EDW in FLAME. As in Fig. 4, but for EDW entrances by (a),(c) warming; (b),(d) cooling; (e),(g) stratification decreases; and (f),(h) layer thickness increases are binned instead of EDW exits.

as the shorter segments expire before the longer segments. To prevent each ensemble-average trajectory from being dominated by the shape of a small subsample of the segments and exhibiting discontinuous jumps, each ensemble-mean trajectory is truncated when there are less than 1000 segments contributing to the average.

Both temporarily in and permanently in EDW particles reside within a region from roughly 25° to 40°N (Fig. 6), 100 to 400 m (Fig. 1b), and potential density $\sigma_\theta = 26.1$ to 26.5 kg m^{-3} (not shown). Binning the EDW segments in depth and density space (not shown) yields the same result as the depth and density ranges cited

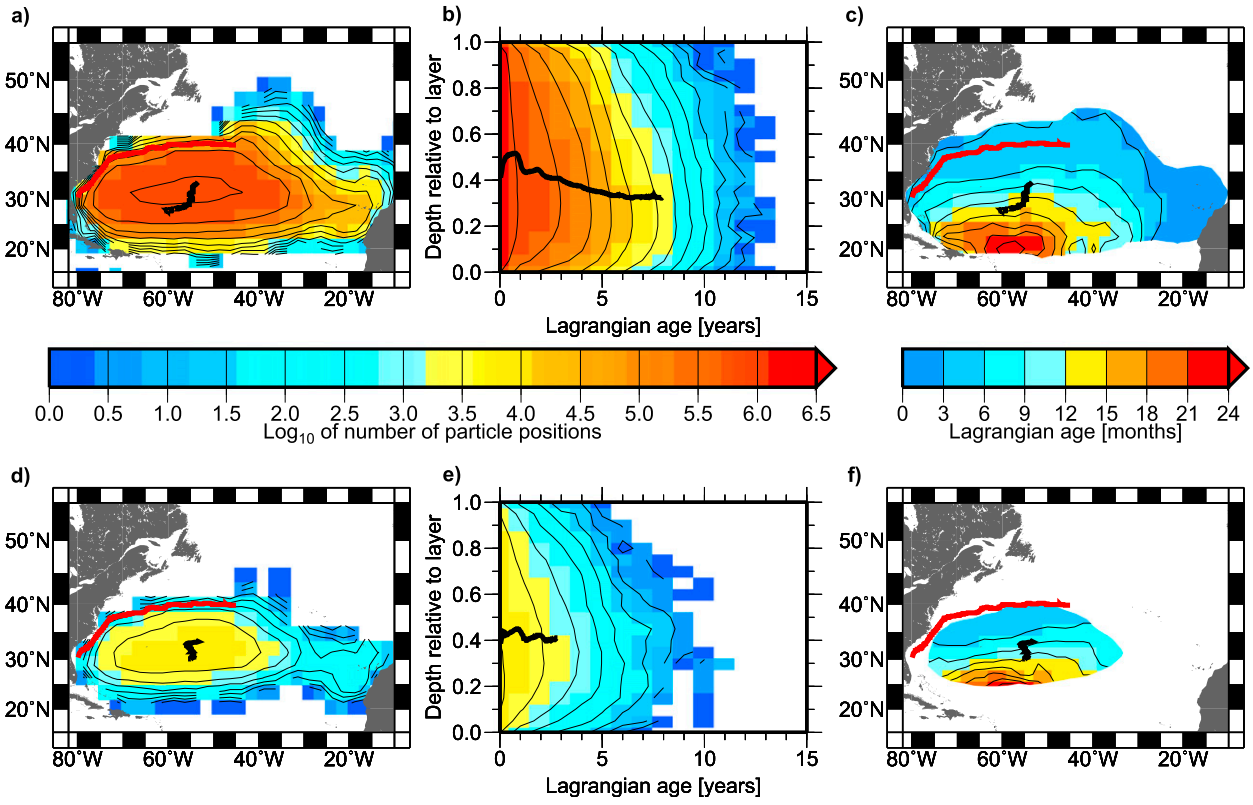

FIG. 6. EDW pathways. (a) Log_{10} of the number of particle positions composing the segments that are temporarily in EDW in each 2.5° × 2.5° box. (b) Log_{10} of the number of particle positions composing the temporarily in EDW segments in each 300 day × 0.05 relative depth box. We use the same definition of particle relative depth as in Figs. 4 and 5. (c) Average Lagrangian age of the temporarily in EDW segments computed for each 2.5° × 2.5° box. The Lagrangian age maps are clipped so that no ages are shown if fewer than 1000 particle positions are found in a bin. (d)–(f) Histograms and age maps for the permanently in EDW segments computed in the same way as (a)–(c). Contour lines are drawn at 0.5 intervals on the $\log_{10}$ scale on histograms or every 3 months for the age maps. The thick black lines are the ensemble-average trajectory clipped at the time step when there are less than 1000 segments remaining in EDW. The red line in the maps is the time-mean position of the north wall of the Gulf Stream, as in Fig. 1.

above. The extent of the modeled EDW is consistent with hydrographic and passive tracer observations (Kwon and Riser 2004; LeBel et al. 2008) and data assimilating model output (Maze et al. 2009; Maze and Marshall 2011), albeit slightly lighter.

In both EDW and non-EDW ensembles, particles follow the large-scale anticyclonic circulation of the subtropical gyre as they gradually sink within the EDW layer. The southward migration of EDW particles is reflected in the Lagrangian age distribution (Figs. 6c,f). Particle ages range from, on average, a couple of months in the northern reaches of the EDW pool (near 35°N) to more than 2 yr in the southern portion of the EDW region (near 20°N). Therefore, on average, the oldest EDW lies to the south of the EDW pool, away from the formation region along the northern boundary of the EDW pool. The first temporarily in EDW segment along the trajectory in Fig. 2 is an example of the oldest EDW.

The temporarily in and permanently in EDW segments exhibit similar behavior because both ensembles are constrained to the EDW pool (Fig. 6). On the other hand, the temporarily out and permanently out EDW segments have different long-term fates. The temporarily out EDW segments (Fig. 7) tend to occupy a similar domain as the EDW segments (Fig. 6) in the horizontal (20°–40°N) and in the vertical (0–500 m), and they have a stable average potential density of about $\sigma_\theta = 26.2\,\text{kg m}^{-3}$, within the EDW density range. The main difference is that the temporarily out segments are spread over a wider range of latitudes, depths, and density classes than the EDW segments and are also slightly more concentrated near the southern and southwestern boundary of the region. Because all the temporarily out EDW segments will eventually return to the EDW pool at the end of the segment, they are also ultimately constrained by the EDW pool.

The permanently out EDW segments do not return to the EDW pool by the end of the simulation. As such, the

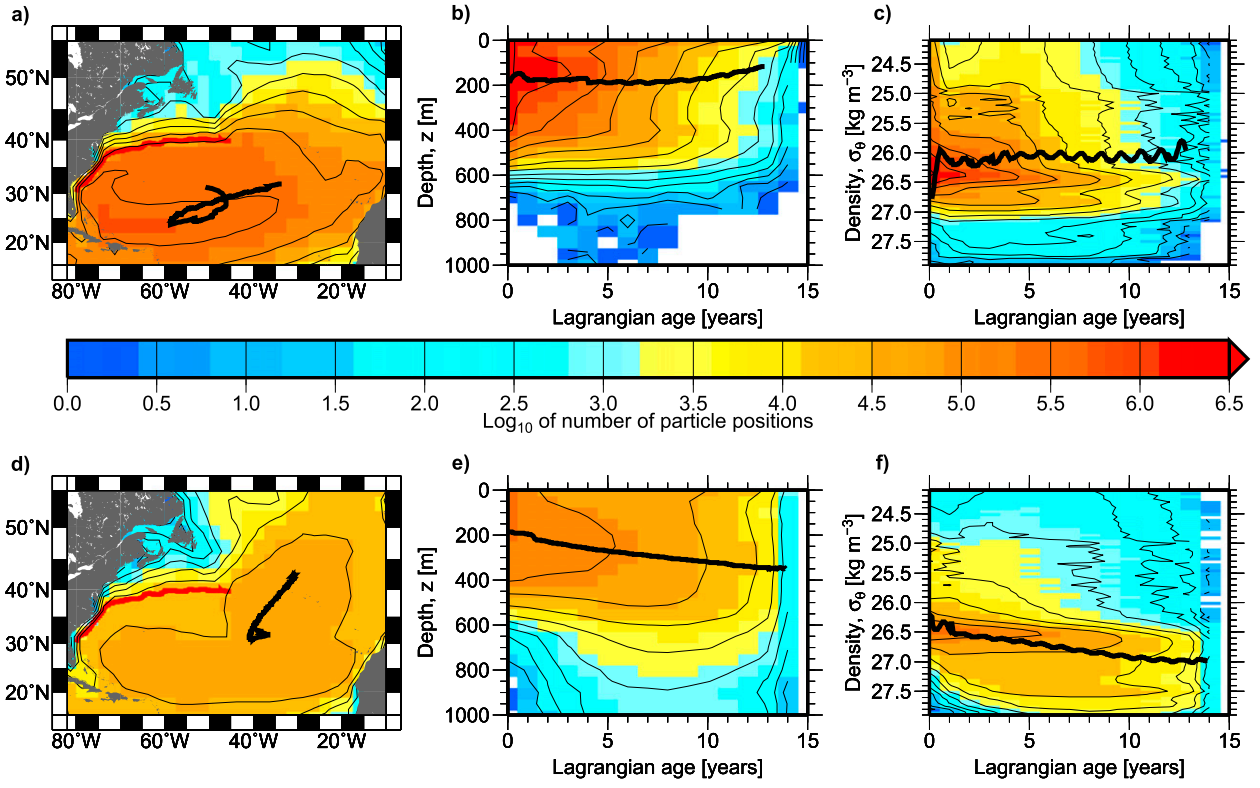

FIG. 7. Non-EDW pathways. (a) Log_{10} of the number of particle positions composing the segments that are temporarily out of EDW in each 2.5° × 2.5° box. (b) Log_{10} of the number of particle positions composing the temporarily out of EDW segments in each 300 day × 40 m bin. Because the particles are out of the EDW layer, the normalized depth relative to layer thickness no longer applies. (c) Log_{10} of the number of particle positions composing the temporarily out of EDW segments in each 300 day × 0.05 kg m^{-3} bin. (d)–(f) Histograms for the permanently out of EDW segments computed in the same way as (a)–(c). Contour lines are drawn at 0.5 intervals on the $\log_{10}$ scale. The thick black lines are the ensemble-average trajectory clipped at the time step when there are less than 1000 segments remaining out of EDW. The red line in the maps is the time-mean position of the north wall of the Gulf Stream, as in Fig. 1.

permanently out segments are exported much farther, go deeper, and experience a net increase in density compared to the temporarily out EDW segments (Fig. 7). Therefore, the permanently out EDW segments represent the long-term fate of EDW as it is mixed into the surrounding waters and exported from the subtropics to the subpolar gyre as part of the larger-scale circulation in the FLAME model.

We note that despite the increased range of non-EDW, the EDW and non-EDW segments do not occupy mutually exclusive domains. Rather, there is overlap in the zones that EDW and non-EDW occupy, reinforcing the observation that the EDW domain contains patches of the surrounding non-EDW (Fig. 3). The similarities between temporarily in segments and temporarily out segments are also reflected in the particle residence times. Figure 8 shows the number of temporarily in and temporarily out particles. Because Fig. 8 is plotted with a $\log_{10}$ scale, more than 70% of the temporarily in and temporarily out EDW segments are less than a year long. For the duration of the simulation, the number of particles remaining within EDW can be approximated with a decaying exponential whose *e*-folding time is about 1 yr (Fig. 8). In addition, on time scales of about a year or less, the temporarily out EDW particles return to EDW with an *e*-folding time scale of about 1 yr (Fig. 8). Because these *e*-folding time scales are similar, temporarily in EDW particles are leaving EDW as temporarily out EDW particles return. However, on time scales greater than 1 yr, the *e*-folding time of the temporarily out particles becomes much longer as the temporarily out particles move farther away from EDW and thus take much longer to return to EDW.

c. *Dynamical constraints on Lagrangian pathways*

In this section, we verify that the initial southward migration of particles within EDW and the eventual export of particles out of EDW into the surrounding waters of the subtropical gyre and toward the subpolar gyre are consistent with the structure of the large-scale density field. Our discussion will focus on the potential vorticity q of EDW and the surrounding waters. Here,

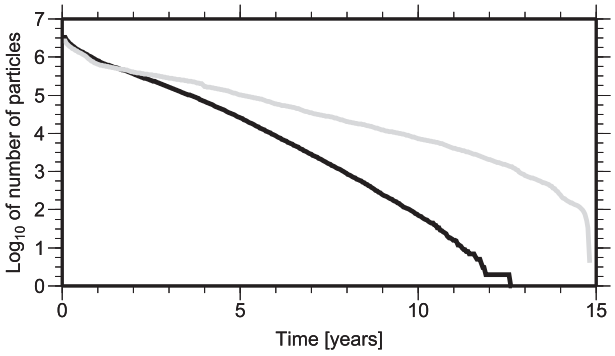

FIG. 8. Time scales of EDW and non-EDW pathways. The number of particles remaining in the temporarily in (black) and temporarily out (gray) EDW ensembles is plotted on a $\log_{10}$ scale with respect to the Lagrangian age of each particle. The resolution of each curve is at 15-day steps, the same as the frequency of trajectory position updates.

we use the layer definition of potential vorticity $q = (\zeta + f)/h$, where f is the Coriolis parameter, ζ is the local vorticity, and h is the thickness of the layer. Consistent with standard scaling arguments, ζ is an order of magnitude less than f outside of the boundary currents in FLAME (not shown), so we present only f/h in maps of q (Fig. 9).

Potential vorticity is a conserved quantity and it can be broken into mean and eddy quantities (e.g., Rhines and Holland 1979):

$$\frac{D\overline{q}}{Dt} = \overline{\mathbf{u}} \cdot \nabla \overline{q} = -\nabla \cdot \overline{\mathbf{u}'q'} + \overline{F} - \overline{\Delta},$$

where q' and $\mathbf{u}'$ are the eddy deviations with respect to the time mean $\overline{q}$ and velocity $\overline{\mathbf{u}}$. The sources and sinks of q are described by F and Δ, the forcing and dissipation, respectively. In the absence of eddies, forcing, and dissipation, contours of mean potential vorticity coincide with contours of the mean streamfunction. However, in FLAME, the mean flow in the EDW pool crosses potential vorticity contours, suggesting an active role for either eddies or forcing and/or dissipation (Fig. 9b).

Forcing and dissipation obviously play a large role where the EDW layer outcrops to the surface. EDW is directly exposed to the atmosphere during the winter and separated from the atmosphere in the summer so there are seasonal sources and sinks of q in EDW in the region where EDW outcrops (i.e., Maze and Marshall 2011). On the other hand, the southernmost extent of the winter 20°C outcrop in FLAME is on average between 25° and 30°N (Fig. 1), so a significant fraction of the EDW pool is effectively isolated from direct, local forcing. The anticyclonic circulation of the EDW layer means that in the vicinity of where EDW outcrops, north of about 30°N, $\overline{\mathbf{u}} \cdot \nabla \overline{q} < 0$ (Fig. 9b) because the direction of the mean velocity (southeastward) is against the direction of the mean q gradient (northward). This negative potential vorticity tendency is consistent with the observation that over an annual cycle, the net effect of the wind and buoyancy forcing on EDW is to decrease q (Maze and Marshall 2011), hence the anomalously low stratification of EDW compared to the surrounding waters.

In contrast to the outcropped region, within the subducted EDW, $\overline{\mathbf{u}} \cdot \nabla \overline{q} > 0$ because the potential vorticity gradient (southward) is with the direction of the mean flow (southwestward). The change in sign in the mean potential vorticity tendency term suggests that a convergence of eddy fluxes of q plays an important role in the q budget (Fig. 9b). The layer below EDW, where the large-scale homogenization of potential vorticity is evidence for the sustained effect of eddies (McDowell et al. 1982; Rhines and Young 1982), $\overline{\mathbf{u}} \cdot \nabla \overline{q} > 0$ (Fig. 9d). Furthermore, as noted by McDowell et al. (1982), for densities less than $\sigma_\theta = 27.0\,\mathrm{kg\,m^{-3}}$, the meridional q gradient from about 20° to 30°N is southward, while below $\sigma_\theta = 27.0\,\mathrm{kg\,m^{-3}}$ the q gradient is northward. A change in the sign of the meridional q gradient with depth is a classic necessary condition for baroclinic instability. Therefore, the southern reaches of the EDW pool are potentially unstable. This instability could be the source of eddies, and it is possible that a mean flow is driven southward across mean q contours by eddies.

Finally, the long-term export of EDW away from the subtropical gyre is consistent with the results of Burkholder and Lozier (2011), who propose that the export of waters from the subtropical to subpolar gyres is dominated by subsurface flow. In particular, they show that Lagrangian particles launched at several hundred meters depth in the FLAME model are more likely to be exported from the subtropical to the subpolar gyre than particles with shallow launch locations. The movement of permanently out EDW in the horizontal plane and in density space (Figs. 7d,f) illustrates this export pathway. The permanently out EDW segments, initially strongly focused in the $\sigma_\theta = 26.5$–$27.0\,\mathrm{kg\,m^{-3}}$ density range, sink to the $\sigma_\theta = 27.3$–$27.6\,\mathrm{kg\,m^{-3}}$ range as the particles move from the subtropical to the subpolar gyre. This density class matches the range that McDowell et al. (1982) identify as the shallowest layer that allows free communication between the subpolar and subtropical gyres, consistent with the potential vorticity field in an updated hydrographic climatology and the FLAME model (Figs. 9g,h).

d. EDW time scales in a Lagrangian frame

In the previous sections, our focus was on the fate of particles launched in EDW. In this section we examine

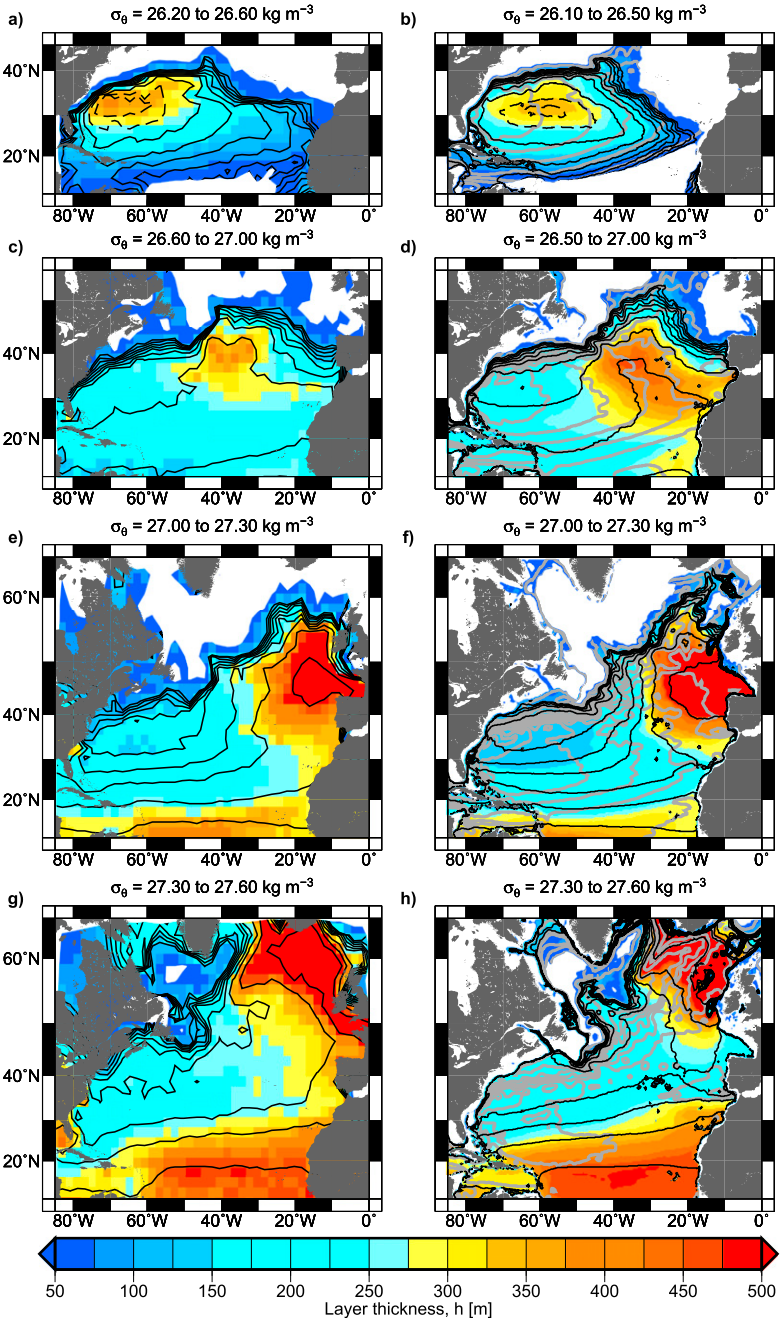

FIG. 9. Structure of the EDW and below EDW density field. Climatological-average thickness between the (a) σ_θ = 26.20–26.60 kg m^{-3}, (c) σ_θ = 26.60–27.00 kg m^{-3}, (e) σ_θ = 27.00–27.30 kg m^{-3}, and (g) σ_θ = 27.30–27.60 kg m^{-3} isopycnal layers in the hydrographic climatology. (b),(d),(f),(h) Corresponding isopycnal layers in the FLAME model, with slightly lighter values for the top two layers compared to the observations. The average layer potential vorticity f/h is contoured at 1×10^{-7} m^{-1} s^{-1} (solid black) and 2.5×10^{-8} m^{-1} s^{-1} (dashed black) intervals. In (b), (d),(f), and (h), the gray lines are streamlines at 1.5×10^4, 1.0×10^4, 0.5×10^4, and 0.5×10^4 m^2 s^{-1} contour intervals, respectively, computed from the climatological-average velocity in each respective layer. The observed climatology is computed over all available data, and the FLAME climatological averages are computed over the duration of the model run (1990–2004). The isopycnal surfaces presented here were picked to allow for direct comparisons with the surfaces shown in McDowell et al. (1982). Because the EDW density in FLAME is slightly different than in observations, the density ranges in (b) and (d) are shifted by 0.1 kg m^{-3}.

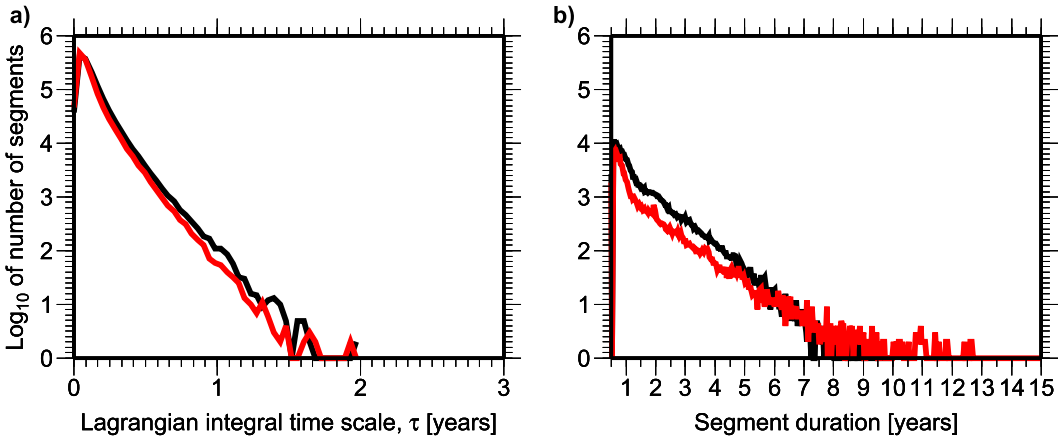

FIG. 10. Persistence of temperature anomalies along particle trajectories. (a) The number of trajectory segments whose integral time scale τ of along-track temperature time series fall into each 15-day bin. The distribution of τ is shown for all segments in EDW (black) and the temporarily out of EDW segments (red). Because the time series are of limited duration, τ is computed as the integral of the lagged autocorrelation function up to the first zero crossing (Lumpkin et al. 2002). (b) The number of trajectory segments for which the first zero crossing of the lagged autocorrelation function is not found for the duration of the segment so τ is not determined. In this case, the total length of each EDW (black) and temporarily out of EDW (red) segment is binned at 15-day resolution. Integral time scales are not computed for segments with durations of less than 6 months because at 15-day resolution, these segments have only about 12 points.

the fate of EDW properties, namely, the duration of temperature or stratification anomalies along trajectories. We also consider the turnover time of EDW measured in a Lagrangian frame.

Lagrangian temperature anomalies are computed by subtracting the appropriate climatological monthly value from the instantaneous temperature along a trajectory segment based on the date and position along the particle path. Therefore, these anomalies take into account both the seasonal cycle and the spatial structure of the model climatology as the particles change position. Along-track stratification, density, and potential vorticity anomalies are found in the same process as temperature anomalies.

The distribution of integral time scales τ computed for temperature along each EDW segment is shown in Fig. 10a. The τ distributions for anomalies of $\partial T/\partial z$, density, and potential vorticity are very similar to the distributions for temperature and are therefore omitted for brevity. The majority of trajectory segments, both in and out of EDW, have integral time scales of ~3 months or less. Although they are in the minority, there are trajectory segments whose temperature anomaly time series exhibit continuously positive autocorrelations even after lags of several years (Fig. 10b). It is interesting to note that the distribution of integral time scales for trajectory segments in EDW and temporarily out of EDW are nearly identical, but EDW segments exhibit slightly longer integral time scales than non-EDW segments. Averaging over the integral time scales of the 1.35×10^6 temporarily in segments presented in Fig. 10a and the durations of the 1.71×10^5 temporarily in segments plotted in Fig. 10b results in an estimate for the EDW integral time scale of 3.0 months. Similarly, the average integral time scale for all temporarily out segments is 2.2 months. The longer integral time scale in EDW compared to non-EDW is consistent with the observation that EDW properties are more homogeneous compared to the surrounding non-EDW.

We also searched for, and did not find, a clear relationship between the initial magnitude of each anomaly and the duration of that anomaly along the particle path. Furthermore, we also did not find any strong indication that the initial and final anomalies of EDW segments are correlated. These negative results indicate that anomalies along individual particle paths are subsumed by the surrounding waters on time scales of several months, indicating strong physical or numerical mixing.

The integral time scales of individual particles in EDW reported here and their average duration in EDW (~10 months; section 4b) are much shorter than the turnover time (~3 yr; section 3) calculated earlier. Because the Lagrangian particles are widely distributed over the whole of the EDW domain (Fig. 6), and they exhibit a seasonal cycle in their entrances and exits from EDW (Figs. 4, 5), it is also possible to estimate EDW turnover as the ratio of the annual-average number of particles in EDW to the annual change in the number of particles in EDW.

The EDW turnover based on Lagrangian particles is presented in Fig. 11. Figure 11a shows the total number of trajectories in EDW for each season during the trajectory simulation. As explained in section 2d, trajectories

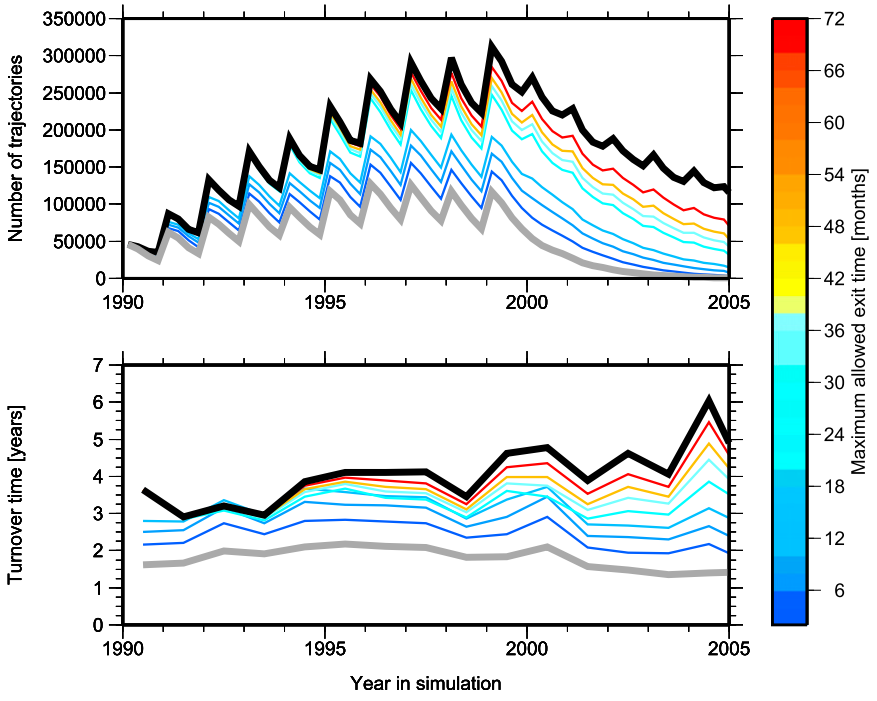

FIG. 11. EDW turnover computed in a Lagrangian frame. (a) Number of trajectories in EDW at each season during the simulation. There are four seasonal time steps per year: February–April (FMA), May–July (MJJ), August–October (ASO), and November–January (NDJ). The start of the time axis corresponds to the winter of 1990 when the first particles are launched. Each following winter (FMA) from 1991 to 1999, more trajectories are initialized (section 2d), so the total number of particles increases substantially each winter. During the rest of each year and once all the particle launches are finished, the number of particles in EDW slowly decreases due to the exiting particles. The black line is the number of all trajectories that are in EDW during each individual season. The gray line corresponds to the case when trajectories are not included in the inventory after their first exit from EDW even if they come back into EDW later on in the simulation. The colored lines are inventories of trajectories in EDW up to the first instance each trajectory exits EDW for a duration greater than the corresponding allowed exit time. (b) The annual turnover time scale corresponding to each curve in (a). The turnover time scale in a Lagrangian frame is computed by dividing the average number of trajectories in EDW for each year by the annual destruction of EDW over each year. The annual destruction of EDW is the difference between the number of trajectories in EDW during the winter and the autumn.

are added to the simulation over the first 10 yr and then advected by the model velocity fields. Therefore, the first ~7 yr of the simulation exhibits a clear growth in the number of trajectories in EDW as particles are distributed from their launch locations throughout the EDW volume. In years 8–10 roughly the same number of particles is added each year, but the total number of particles is more uniform, suggesting that the simulation is approaching a steady state—the number of particles launched in EDW is approximately the same as the number of particles exiting EDW. It is important to note that there are two end-member cases for determining this seasonal inventory: 1) particles that have stayed continuously in EDW since launch and 2) all particles within EDW regardless of previous exits or entries.

Although the average integral time scale of the individual particles is less than a year, the particle ensemble as a whole exhibits turnover time scales of several years (Fig. 11b). Ignoring particles after their first exit results in a turnover time scale of ~2 yr that is approximately the lower bound of our Eulerian estimate of EDW turnover time (3.18 ± 1.06 yr; section 3). Including all possible particles in EDW, even ones that go out of EDW for several years before coming back to EDW, results in a turnover time of ~4 yr, roughly the upper bound on the Eulerian turnover time estimate. Allowing the trajectory inventory to include trajectories with increasing time out of EDW results in a smooth transition between these two end-member cases. Therefore, part of what sets the turnover time scale and its uncertainty is the patchy exchange between EDW and

the surrounding waters. Furthermore, although anomalies are not, on average, carried along individual particle tracks for more than a couple months and the majority of particles in EDW exit after less than 1 yr, the mass movement of those same particles is still reflective of the longer time scale of renewal of EDW, again suggesting a significant role of mixing.

5. Summary and conclusions

The FLAME model is able to simulate EDW with bulk properties, spatial extent, and seasonal cycle consistent with observations. Additionally, the large-scale potential vorticity field in the model compares favorably with the observational record, and simulated particle trajectories are consistent with this potential vorticity field. Therefore, we believe that the results presented here are a reasonable estimate for the envelope of possible EDW pathways in the real ocean.

In the FLAME model, ~90% of EDW exit events are associated with an increase in stratification or decreasing layer thickness. Similarly, particles return to EDW primarily through a decrease in stratification or an increase in layer thickness (~80%). Particle entry and exit based on temperature is less frequent than stratification. However, entries and exits by cooling clearly outweigh entries and exits by warming, consistent with the net average heat flux out of EDW (Grist and Josey 2003; Large and Yeager 2009) and calculations based on surface flux–forced water mass transformation (Maze et al. 2009). Finally, while there are exits from EDW and entries into EDW through the bottom of the EDW layer throughout the course of the year, EDW exits and entries through the top of the EDW layer exhibit a strong seasonal cycle consistent with EDW formation in winter due to strong surface buoyancy forcing and isolation from the surface for the remainder of the year.

A combination of the gyre circulation and an eddy-driven mean flow transports EDW to the south on time scales of a few years in the FLAME model. The majority of EDW particles generally retain their EDW status for less than a year, similar to the integral time scale of non-EDW that occupies the same region. During this time, EDW trajectory subsegments reside in the EDW reservoir from 20° to 40°N and 70° to 40°W and σ_θ = 26.1–26.5 kg m^{-3}. On longer, decadal time scales, EDW and non-EDW recirculate within the subtropical gyre and non-EDW eventually sinks into deeper layers and is exported to high latitudes.

Previous studies (i.e., Kwon and Riser 2004; Forget et al. 2011) estimate an EDW turnover time on the order of several years, which is consistent with the 3.18 ± 1.06 yr EDW turnover time in FLAME. On the other hand, observations of the amount of time it takes for a profiling float in EDW to reenter the mixed layer indicate that 67% of the time EDW reemerges in less than 12 months (Fratantoni et al. 2013). Broadly consistent with these Lagrangian observations, in the FLAME model, 54% (74%) of particles within EDW exit EDW after less than 6 months (12 months), and the average duration of temporarily in EDW segments is about 10 months. A more focused study of the specific reoutcropping behavior of the particles will be presented elsewhere. The key point here is that the majority of simulated Lagrangian floats exit EDW on time scales of less than 1 yr that is substantially less than the ~3 yr turnover time.

In addition to the residence time of particles in EDW being less than 1 yr, the average integral time scale of property anomalies along individual particle trajectories within EDW and outside of EDW is 3.0 and 2.2 months, respectively. The longer integral time scale in EDW compared to non-EDW is consistent with the greater homogeneity of the mode water compared to the surrounding watermasses. However, the property anomaly integral time scales for particles that are in EDW and out of EDW are both substantially less than a year, suggesting a significant role for either physical or numerical mixing.

In contrast to the less than 1-yr time scales of individual particles, the ensemble movement of the EDW particles exhibits a longer turnover time. Estimating the EDW turnover based on the number of trajectories in EDW results in a ~2–4-yr turnover time, which is consistent with the turnover time calculated from the time series of EDW volume. Therefore, although individual particles exhibit comparatively short memories and residence times, the ensemble mass movement of particles is consistent with the longer turnover times. Furthermore, exchange between EDW and the surrounding waters is frequent and makes a significant impact on the turnover time scale.

Acknowledgments. The authors are thankful for financial support from the U.S. National Science Foundation for S. F. G., M. S. L., Y.-O. K., and J. J. P. We are also thankful to Claus Böning (GEOMAR) for generously providing all of the FLAME model output and the original trajectory computation code.

REFERENCES

Alfultis, M. A., and P. Cornillon, 2001: Annual and interannual changes in the North Atlantic STMW layer properties. *J. Phys. Oceanogr.*, **31,** 2066–2086, doi:10.1175/1520-0485(2001)031<2066:AAICIT>2.0.CO;2.

Biastoch, A., C. W. Böning, J. Getzlaff, J.-M. Molines, and G. Madec, 2008: Causes of interannual–decadal variability in the meridional overturning circulation of the midlatitude North Atlantic Ocean. *J. Climate,* **21,** 6599–6615, doi:10.1175/2008JCLI2404.1.

Böning, C. W., and M. D. Cox, 1988: Particle dispersion and mixing of conservative properties in an eddy-resolving model. *J. Phys. Oceanogr.,* **18,** 320–338, doi:10.1175/1520-0485(1988)018<0320:PDAMOC>2.0.CO;2.

——, M. Scheinert, J. Dengg, A. Biastoch, and A. Funk, 2006: Decadal variability of subpolar gyre transport and its reverberation in the North Atlantic overturning. *Geophys. Res. Lett.,* **33,** L21S01, doi:10.1029/2006GL026906.

Boyer, T. P., and S. Levitus, 1997: Objective analyses of temperature and salinity for the world ocean on a 1/4 degree grid. NOAA Atlas NESDIS 11, U.S. Government Printing Office Tech. Rep., 83 pp.

Burkholder, K. C., and M. S. Lozier, 2011: Subtropical to subpolar pathways in the North Atlantic: Deductions from Lagrangian trajectories. *J. Geophys. Res.,* **116,** C07017, doi:10.1029/2010JC006697.

Davis, X. J., F. Straneo, Y.-O. Kwon, K. A. Kelly, and J. M. Toole, 2013: Evolution and formation of North Atlantic Eighteen Degree Water in the Sargasso Sea from moored data. *Deep-Sea Res. II,* **91,** 11–24, doi:10.1016/j.dsr2.2013.02.024.

Dong, S., S. L. Hautala, and K. A. Kelly, 2007: Interannual variations in upper-ocean heat content and heat transport convergence in the western North Atlantic. *J. Phys. Oceanogr.,* **37,** 2682–2697, doi:10.1175/2007JPO3645.1.

Forget, G., G. Maze, M. Buckley, and J. Marshall, 2011: Estimated seasonal cycle of North Atlantic Eighteen Degree Water volume. *J. Phys. Oceanogr.,* **41,** 269–286, doi:10.1175/2010JPO4257.1.

Fratantoni, D. M., Y.-O. Kwon, and B. A. Hodges, 2013: Direct observation of subtropical mode water circulation in the western North Atlantic Ocean. *Deep-Sea Res. II,* **91,** 35–56, doi:10.1016/j.dsr2.2013.02.027.

Fuglister, F. C., and A. D. Voorhis, 1965: A new method for tracking the Gulf Stream. *Limnol. Oceanogr.,* **10,** 115–124.

Gary, S. F., M. S. Lozier, C. W. Böning, and A. Biastoch, 2011: Deciphering the pathways for the deep limb of the meridional overturning circulation. *Deep-Sea Res. II,* **58,** 1781–1797, doi:10.1016/j.dsr2.2010.10.059.

Grist, J. P., and S. A. Josey, 2003: Inverse analysis adjustment of the SOC air–sea flux climatology using ocean heat transport constraints. *J. Climate,* **16,** 3274–3295, doi:10.1175/1520-0442(2003)016<3274:IAAOTS>2.0.CO;2.

Hanawa, K., and L. Talley, 2001: Mode waters. *Ocean Circulation and Climate,* J. Siedler, J. Church, and J. Gould, Eds., International Geophysics Series, Vol. 77, Academic Press, 373–386.

Hüttl-Kabus, S., and C. W. Böning, 2008: Pathways and variability of the off-equatorial undercurrents in the Atlantic Ocean. *J. Geophys. Res.,* **113,** C10018, doi:10.1029/2007JC004700.

Jenkins, W. J., 1988: The use of anthropogenic tritium and helium-3 to study subtropical gyre ventilation and circulation. *Philos. Trans. Roy. Soc. London,* **A325,** 43–61, doi:10.1098/rsta.1988.0041.

Joyce, T. M., 2012: New perspectives on Eighteen-Degree Water formation in the North Atlantic. *J. Oceanogr.,* **68,** 45–52, doi:10.1007/s10872-011-0029-0.

——, L. N. Thomas, and F. Bahr, 2009: Wintertime observations of subtropical mode water formation within the Gulf Stream. *Geophys. Res. Lett.,* **36,** L02607, doi:10.1029/2008GL035918.

Kalnay, E. M., and Coauthors, 1996: The NCEP/NCAR 40-Year Reanalysis Project. *Bull. Amer. Meteor. Soc.,* **77,** 437–471, doi:10.1175/1520-0477(1996)077<0437:TNYRP>2.0.CO;2.

Kelly, K. A., R. J. Small, R. M. Samelson, B. Qiu, T. M. Joyce, Y.-O. Kwon, and M. Cronin, 2010: Western boundary currents and frontal air–sea interaction: Gulf Stream and Kuroshio Extension. *J. Climate,* **23,** 5644–5667, doi:10.1175/2010JCLI3346.1.

Klein, B., and N. Hogg, 1996: On the variability of 18 Degree Water formation as observed from moored instruments at 55°W. *Deep-Sea Res. I,* **43,** 1777–1806, doi:10.1016/S0967-0637(96)00069-6.

Kwon, Y.-O., and S. C. Riser, 2004: North Atlantic Subtropical Mode Water: A history of ocean–atmosphere interaction 1961–2000. *Geophys. Res. Lett.,* **31,** L19307, doi:10.1029/2004GL021116.

Large, W. G., and S. G. Yeager, 2009: The global climatology of an interannually varying air–sea flux data set. *Climate Dyn.,* **33,** 341–364, doi:10.1007/s00382-008-0441-3.

LeBel, D. A., and Coauthors, 2008: The formation rate of North Atlantic Deep Water and Eighteen Degree Water calculated from CFC-11 inventories observed during WOCE. *Deep-Sea Res. I,* **55,** 891–910, doi:10.1016/j.dsr.2008.03.009.

Levitus, S., and T. P. Boyer, 1994: *Temperature.* Vol. 4, *World Ocean Atlas 1994,* NOAA Atlas NESDIS 4, 117 pp.

——, R. Burgett, and T. P. Boyer, 1994: *Salinity.* Vol. 3, *World Ocean Atlas 1994,* NOAA Atlas NESDIS 3, 99 pp.

Lozier, M. S., W. B. Owens, and R. G. Curry, 1995: The climatology of the North Atlantic. *Prog. Oceanogr.,* **36,** 1–44, doi:10.1016/0079-6611(95)00013-5.

Lumpkin, R., A.-M. Treguier, and K. Speer, 2002: Lagrangian eddy scales in the northern Atlantic Ocean. *J. Phys. Oceanogr.,* **32,** 2425–2440, doi:10.1175/1520-0485-32.9.2425.

Maze, G., and J. Marshall, 2011: Diagnosing the observed seasonal cycle of the Atlantic Subtropical Mode Water using potential vorticity and its attendant theorems. *J. Phys. Oceanogr.,* **41,** 1986–1999, doi:10.1175/2011JPO4576.1.

——, G. Forget, M. Buckley, and J. Marshall, 2009: Using transformation and formation maps to study the role of air–sea heat fluxes in North Atlantic Eighteen Degree Water formation. *J. Phys. Oceanogr.,* **39,** 1818–1835, doi:10.1175/2009JPO3985.1.

McDowell, S., P. B. Rhines, and T. Keffer, 1982: North Atlantic potential vorticity and its relation to the general circulation. *J. Phys. Oceanogr.,* **12,** 1417–1436, doi:10.1175/1520-0485(1982)012<1417:NAPVAI>2.0.CO;2.

National Oceanographic Data Center, cited 2012: World Ocean database. [Available online at http://www.nodc.noaa.gov/OC5/SELECT/dbsearch/dbsearch.html.]

Pacanowski, R. C., 1996: MOM2 version 2.0 (beta) documentation, user's guide, and reference manual. GFDL Ocean Tech. Rep. 3.2, 350 pp. [Available online at http://gfdl.noaa.gov/cms-filesystem-action/model_development/ocean/manual2.2.pdf.]

Palter, J. B., M. S. Lozier, and R. T. Barber, 2005: The effect of advection on the nutrient reservoir in the North Atlantic subtropical gyre. *Nature,* **437,** 687–692, doi:10.1038/nature03969.

Rhines, P. B., and W. R. Holland, 1979: A theoretical discussion of eddy-driven mean flows. *Dyn. Atmos. Oceans,* **3,** 289–325, doi:10.1016/0377-0265(79)90015-0.

——, and W. R. Young, 1982: Homogenization of potential vorticity in planetary gyres. *J. Fluid Mech.,* **122,** 347–367, doi:10.1017/S0022112082002250.

Siedler, G., A. Kuhl, and W. Zenk, 1987: The Madeira Mode Water. *J. Phys. Oceanogr.,* **17,** 1561–1570, doi:10.1175/1520-0485(1987)017<1561:TMMW>2.0.CO;2.

Silverthorne, K. E., and J. M. Toole, 2013: Quasi-Lagrangian observations of the upper ocean response to wintertime forcing in the Gulf Stream. *Deep-Sea Res. I,* **91,** 25–34, doi:10.1016/j.dsr2.2013.02.021.

Speer, K., and E. Tziperman, 1992: Rates of water mass formation in the North Atlantic Ocean. *J. Phys. Oceanogr.,* **22,** 93–104, doi:10.1175/1520-0485(1992)022<0093:ROWMFI>2.0.CO;2.

Talley, L. D., and M. E. Raymer, 1982: Eighteen Degree Water variability. *J. Mar. Res.,* **40,** 757–775.

Worthington, L., 1958: The 18°C water in the Sargasso Sea. *Deep-Sea Res.,* **5,** 297–305, doi:10.1016/0146-6313(58)90026-1.

——, 1976: *On the North Atlantic Circulation*. Johns Hopkins University Press, 110 pp.